Available online at www.sciencedirect.com
ScienceDirect
Geochimica et Cosmochimica Acta 72 (2008) 1837–1847
Geochimica et Cosmochimica Acta
www.elsevier.com/locate/gca

Effects of layer-charge distribution on the thermodynamic and microscopic properties of Cs-smectite

Xiandong Liu, Xiancai Lu *, Rucheng Wang, Huiqun Zhou

State Key Laboratory for Mineral Deposit Research, Department of Earth Sciences, Nanjing University, Nanjing 210093, PR China

Received 4 September 2007; accepted in revised form 24 January 2008; available online 13 February 2008

Abstract

To explore the effects of layer-charge distribution on the thermodynamic and microscopic properties of Cs-smectites, classical molecular dynamic simulations are performed to derive the swelling curves, distributions and mobility of interlayer species, and Cs binding structures. Three representative smectites with distinct layer-charge distributions are used as model clay frameworks and interlayer water content is set within a wide range from 0 to 380 mg_{water}/g_{clay}. All the three smectites swell in a similar way, presenting the characteristic swelling plateaus and similar trends of swelling energetic profiles. The full-monolayer hydrate, corresponding to the global minima of the immersion energy, is the most stable hydrated state of Cs-smectites. The calculated diffusion coefficients of interlayer species disclose the confining effects in all smectites: both water molecules and ions diffuse slower than corresponding bulk cases and they are much more mobile in the direction parallel to the clay surfaces than perpendicular to them. The formed inner-sphere complex structures are very similar in different smectites: ions bind on the H-sites or T-sites and water molecules form cage-like caps covering the ions. Layer-charge distribution is found to have significant influences on the mobility of interlayer species and preference of ion binding sites. A general sequence is proposed to elucidate the preferences of various hexagonal sites (H-sites) and triangular sites (T-sites), that is, tetrahedrally substituted H-sites > nonsubstituted H-sites > tetrahedrally substituted T-sites > nonsubstituted T-sites, but the influence of octahedral substitutions on the preference of the neighboring sites is not obvious. Analysis of mobility indicates that H-sites are more stable Cs-fixation positions than T-sites and smectite with higher fraction of octahedral charges seems to be the most effective barrier material no matter how water content varies although all smectites can immobilize Cs ions in relatively dry conditions. These findings will not only facilitate basic research in geochemistry and material sciences, but also promote the barrier material designing.

1. INTRODUCTION

The basic structure of smectite is the "T-O-T" layer consisting of an octahedral sheet sandwiched by two tetrahedral sheets (Grim, 1962; Brindley and Brown, 1980; Bleam, 1993). Isomorphic substitutions in octahedral and/or tetrahedral sheets commonly make the clay platelets negatively charged, which are compensated by interlayer ions. Water and other polar solvents can enter interlayer regions and cause clay-swelling, and water is found to be able to form integer-number molecular layers in smectite hydrates (Mooney et al., 1952a,b; Boek et al., 1995; Skipper et al., 1995a,b; Karaborni et al., 1996; Skipper, 1998; Skipper et al., 2006). These properties make smectites important in many geological processes and industrial applications (Grim, 1962; Bleam, 1993). Smectites have been widely used as adsorbents in environmental engineering and the barrier materials to fix radioactive nuclides in nuclear waste disposal. Among various radioactive nuclides, ^{134}Cs and ^{137}Cs are especially dangerous being long half-lives and high bioavailability (Evans et al., 1983; Cho et al., 1993; Cornell, 1993). Bentonite, mainly consisting of smectites (mostly montmorillonite and also others, e.g. beidellite

* Corresponding author. Fax: +86 25 83686016.
E-mail address: xcljun@nju.edu.cn (X. Lu).

0016-7037/$ - see front matter © 2008 Elsevier Ltd. All rights reserved.
doi:10.1016/j.gca.2008.01.028

and nontronite), has been found very suitable to adsorb and fix Cs ions in interlayer spaces, and hence suitable to be used as barrier to separate nuclear wastes from the host environment in disposal sites (Onodera et al., 1998). So, low mobility of Cs ions in the interlayer space of smectites is prerequisite.

Although some previous investigations have focused on Cs-smectite, some issues remain open especially on the microscopic structural and dynamic properties. It has been suggested that a Cs-smectite hydrate with water less than one-half monolayer holds stably even under high humidity and that additional water adsorbs in interparticle micropores but not in interlayer spaces (Calvet, 1972; Sutton and Sposito, 2001). But others argued that the full-monolayer hydrate is the most stable state based on molecular simulation investigations (Smith, 1998; Young and Smith, 2000; Whitley and Smith, 2004). Although it is accepted that Cs ion prefers binding on phyllosilicate surfaces, the binding mechanism and the coordination states are still not well understood (Schlegel et al., 2006). It is deduced that layer-charge distribution can influence the physical and chemical properties of Cs-smectites (Weiss et al., 1990; Kim et al., 1996; Onodera et al., 1998), but neither the mechanism nor the extent of this influence has been pictured yet. Onodera et al. (1998) reported that the residual Cs amount after Ba^{2+}-exchange correlates well with octahedral charges, but the underlying mechanisms are blurred by the complexity involved in the cation exchange process (Teppen and Miller, 2006).

In the past decade, molecular dynamics (MD) simulation has been widely employed to study the clay-fluid systems and many good agreements with experiments have been reached (He et al., 2005; Skipper et al., 2006 and references therein). However, previous simulations of Cs-smectites cannot distinguish the effects of layer-charge distributions sufficiently due to the disability of their force fields to treat different isomorphic substitutions (Smith, 1998; Young and Smith, 2000; Sutton and Sposito, 2001, 2002; Masashi et al., 2003; Whitley and Smith, 2004). In this study, we carried out comprehensive MD simulations on Cs-smectites with a wide range of water contents in order to obtain thermodynamic and microscopic properties of Cs-smectite and to disclose the effects of layer-charge distributions. Three representative smectites with different isomorphic substitutions were selected as model smectites and the advanced *clayff* force field (Cygan et al., 2004b) was employed. Swelling curves, swelling thermodynamics, spatial distributions, mobility of Cs ions and interlayer water, and microscopic structure were derived. Extensive comparisons show that the swelling behaviors and confining effects of the interspaces are similar for the three smectites. Effects of isomorphic substitutions on the mobility of interlayer species and distributions of surface binding sites were revealed in detail.

2. METHODOLOGY

2.1. Model smectites

Three smectites including Arizona-type montmorillonite (Ari), Wyoming-type montmorillonite (Wyo) and beidellite (Bei) (Sutton and Sposito, 2001; Tambach et al., 2004a,b) were selected in this study for their layer-charge distributions are distinctly different, i.e. Ari only bears octahedral charges, Bei only has tetrahedral charges, and Wyo has both types. Table 1 displays their chemical formulae, cation exchange capacities (CECs) and layer-charge distributions. In this paper, nonsubstituted triangular site (T_n) and substituted triangular site (T_t) represent the T-sites above the tetrahedral silicon and tetrahedral aluminum, respectively. H_t denotes the H-site adjacent to a tetrahedral aluminum atom and H_n stands for other H-sites. The isomorphic substitutions obey Loewenstein's rule (Loewenstein, 1954), i.e. two substitution sites cannot be adjacent. The simulation cell consists of two clay platelets of eight unit cells each: 2 in *x*-dimension and 4 in *y*-dimension and the system contains two interlayer spaces. Thence there are 8, 6 and 6 Cs ions in each interlayer region of the Ari, Wyo and Bei models, respectively. It has been proved the current model is large enough to avoid finite size effects (Chávez-Páez et al., 2001). The basal surface area is about 21.12×18.28 Å^2 and the thickness of a clay sheet is 6.56 Å (Fig. 1(A)). In the simulations, the periodic boundary condition is imposed on three dimensions.

2.2. Simulation details

All molecular dynamics simulations were undertaken by using the *LAMMPS* package (version 10 Nov_2005) (Plimpton, 1995), and *clayff* force field was used to describe the interatomic interactions. *Clayff* assigns partial charges of different coordinating oxygen accurately and distinguishes tetrahedral and octahedral substituting atoms in detail, which makes *clayff* superior for addressing the effects of different substitutions. This force field incorporates the flexible version of the SPC model to describe water molecules (Berendsen et al., 1981; Teleman et al., 1987). *Clayff* has been widely used in geochemical and material simulations, and has shown a wonderful performance (Wang et al., 2004, 2006; Cygan et al., 2004a,b; Greathouse and Cygan, 2005; Kirkpatrick et al., 2005; Liu and Lu, 2006).

Table 1
Chemical formulae, CECs and layer-charge distributions of the model smectites

Model	Chemical formula	CEC (meq/100 g)	Tetrahedral charge (%)	Octahedral charge (%)
Ari (Arizona-type montmorillonite)	$Cs[Si_8][Al_3Mg]O_{20}(OH)_4$	117.6	0	100
Wyo (Wyoming-type montmorillonite)	$Cs_{0.75}[Si_{7.75}Al_{0.25}][Al_{3.5}Mg_{0.5}]O_{20}(OH)_4$	91.7	33.33	66.67
Bei (beidellite)	$Cs_{0.75}[Si_{7.25}Al_{0.75}][Al_4]O_{20}(OH)_4$	91.6	100	0

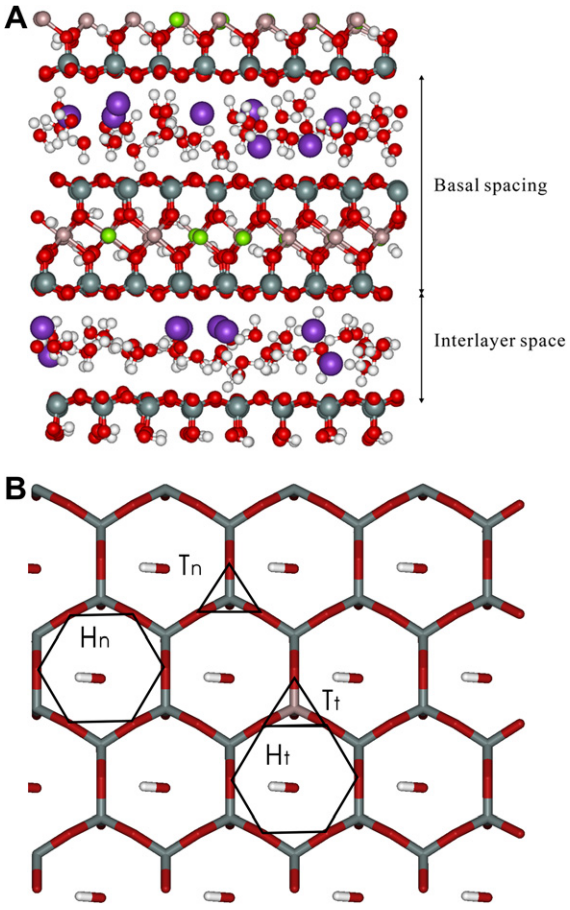

Fig. 1. (A) Snapshot of Ari with water content of approximately 110 mg_{water}/g_{clay}. (B) Illustration of different binding sites. T_n: nonsubstituted triangular site; T_t: substituted triangular site; H_t: hexagonal site adjacent to a tetrahedral aluminum atom; H_o: hexagonal site above an octahedral magnesium atom (not denoted); H_n: other hexagonal site rather than H_t and H_o. Cation Cs = purple, atom O = red, H = white, Si = grey, Al = faded pink and Mg = green. (For interpretation of the references to color in this figure legend, the reader is referred to the web version of this paper.)

In *clayff*, the total energy can be expressed as (Cygan et al., 2004b),

$$E_{total} = E_{Coul} + E_{VDW} + E_{bond\ stretch} + E_{angle\ bend} \quad (1)$$

where E_{Coul} means the long-range coulombic interaction and E_{VDW} stands for the short-range interaction referred to as the Van der Waals term. $E_{bond\ stretch}$ and $E_{bond\ bend}$ denote the bond stretch and bond bend terms, which are given as the simple harmonic forms. A 9.0 Å cut-off is used for the short-range interaction. The coulombic interaction is treated using the Ewald summation (Frenkel and Smit, 1996) and the number of *k*-space vectors is determined to reach a precision of 1.0e−4 in conjunction with the pairwise calculation within a cut-off of 9.0 Å.

In order to study the swelling behaviors of Cs-smectites, we performed 15 simulations for each model, with water content increasing from 0 to about 380 mg_{water}/g_{clay}. As the initial state, ions were placed near the midplane of each interlayer region and water molecules were put randomly in each interlayer space. NPT (298 K, 1 atm) simulations were performed in two stages, firstly an equilibrium stage for 500 ps and then a following production stage for 500 ps to record the results. In these NPT simulations, the *z*-component of the simulation cell was allowed to vary and the other two were fixed.

In determining the swelling curves, three representative water contents of approximately 55, 110 and 380 mg_{water}/g_{clay} were selected to study the structural and dynamical behaviors of interlayer species. These water contents correspond to 20, 40 and 140 water molecules in each interlayer of simulated clay model, respectively. As shown by comparison between the simulated and experimental swelling curves (Section 3.1), the case with water content of about 110 mg_{water}/g_{clay} represents the most stable monolayer hydrate, i.e. the usual form of Cs-smectite in water-rich environment while the case of 55 mg_{water}/g_{clay} was used to mimic the relatively dry condition. The interlayer space of the smectite with the water content of 380 mg_{water}/g_{clay} can be regarded as a broad slit-like pore and was used as an analogy of inter-particle packed pore constructed by two opposite clay sheets in aqueous solutions (Wang et al., 2004; Skipper et al., 2006). For these calculations, a further 500 ps NVT simulation was performed following the previous 1000 ps simulation. A time step of 1.0 fs was used for all cases and the interval of 100 fs for recording trajectories.

2.3. Simulation analyses

The basal spacing value (b) is calculated by averaging the dumping box volume during the production NPT steps,

$$b = \langle V \rangle / (2 \times S) \quad (2)$$

Here $\langle V \rangle$ means the statistically averaged volumes and S is the basal surface area.

Swelling thermodynamic is described by using the immersion energy and hydration energy (Smith, 1998; Boek et al., 1995). The immersion energy is defined as,

$$Q = \langle U(N) \rangle - \langle U(N^0) \rangle - (N - N^0) U_{bulk} \quad (3)$$

where $\langle U(N) \rangle$ stands for the average potential energy of the smectite hydrate with water content N, N^0 is water content of the selected reference state and U_{bulk} is the internal energy of bulk water. In this study we select the state with the highest water content as the reference state for the three smectites. The hydration energy is calculated as,

$$\Delta U = (\langle U(N) \rangle - \langle U(0) \rangle)/N \quad (4)$$

Here $\langle U(0) \rangle$ means the average potential energy of the dry clay. The energy values used in Eqs. (2) and (3) are taken from the production NPT simulations.

The spatial distributions of interlayer species are characterized by the atomic density profiles in the z direction (perpendicular to the clay surface), which are calculated by averaging over the trajectories from the NVT simulations. Taking the plane defined by the average bottom octahedral oxygen positions in Fig. 1 as the origin ($z = 0$), the atomic density reads,

$$\rho(z) = \langle N(z - \Delta z/2, z + \Delta z/2) \rangle / (\Delta z \times S) \quad (5)$$

Here $\langle N(z-\Delta z/2,z+\Delta z/2)\rangle$ is the averaged atom number locating in the height interval of $(z-\Delta z/2,z+\Delta\ z/2)$.

The self-diffusion coefficients D of the interlayer water and ions are calculated according to the Einstein relation (Allen and Tildesley, 1987; Chang et al., 1997),

$$\frac{1}{N}\sum_{i=1}^{N}\langle|\mathbf{r}_i(t)-\mathbf{r}_i(0)|^2\rangle = 2dDt \tag{6}$$

where N is the number of atoms of interest and $\boldsymbol{r}_i(t)$ is the center-of-mass position of the ith one at time t; d is the diffusion dimension, that is, $d=3$ for the total coefficient and $d=1$ for the component coefficient on the separate x, y, or z direction. The left-hand side of Eq. (6) is usually termed as mean squared displacement (MSD).

Cs ion in interlayer pores tends to form inner-sphere complexes by binding to clay surface and the hexagonal site (H-site) and the triangular site (T-site) are main binding sites (Weiss et al., 1990; Kim et al., 1996; Smith, 1998; Ebina et al., 1999). The occupations of different binding sites are derived from the simulation trajectories. All the binding sites are further classified according to layer charge locations (Fig. 1(B)). Cs ions can also form outer-sphere complexes and enter diffuse layer (Bostick et al., 2002; Masashi et al., 2003) and those sites far away from the clay surface are all denoted as "O" for short.

3. RESULTS AND DISCUSSIONS

3.1. Swelling behaviors

Fig. 2 illustrates the derived swelling curves compared with Calvet's experimental measurements. The three simulated curves are very similar and no significant difference is observed. A plateau is presented on each curve as water content is lower than 110 mg_{water}/g_{clay}, which agrees well with previous XRD analysis. Table 2 summarizes the basal spacing values of dry smectites and the plateaus from both simulations and measurements in literature. It can be seen that our simulations agree with experiments fairly well.

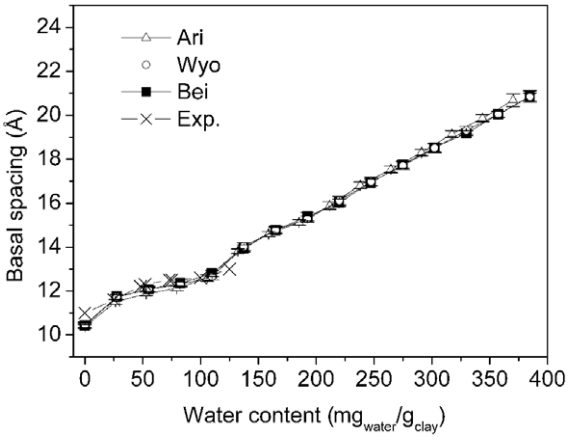

Fig. 2. Cs-smectites swelling curves from the simulations and experimental measurements (Exp.) of Calvet (1973). In most cases, the error bars are smaller than the symbol size.

After the plateau, the basal spacings increase linearly without any stepwise manner as water content increases.

Figs. 3 and 4 display the calculated immersion energy and hydration energy curves. In the immersion energy curves, the global minima are clearly presented at about 110 mg_{water}/g_{clay} and the local minima are at about 220 mg_{water}/g_{clay}. On each hydration energy curve (Fig. 4), one distinct minimum locates at about 110 mg_{water}/g_{clay} and the local one occurs between about 170 and 250 mg_{water}/g_{clay}. The hydration energy is comparable with the calorimetric measurement renormalized by adding the condensation heat of water (−43.9 kJ/mol) (Chang et al., 1995, 1998; Skipper et al., 1995a,b). The global minima of the simulated hydration energy curves are from −47.6 kJ/mol (±2.8 kJ/mol) to −45.0 kJ/mol (±3.0 kJ/mol), and they are very close to the range of calorimetric measurements: $-48.9\sim-46.5$ kJ/mol (approximately $105\sim130$ mg_{water}/g_{clay}) (Bérend et al., 1995). The above good agreement between the measurements and our simulation provides a reliable basis for further analysis. Since the swelling curves and the energy profiles of three smectites present similar trends, it is considered that the mode of isomorphic substitution does not significantly affect the swelling behaviors of Cs-smectites.

It has been found that the energy contribution dominates the swelling free energy, and that the entropy term only serves as a secondary role. The local minima on the swelling immersion energy curve can be used to specify the possible stable hydrate states, and the energy differences of these minima can indicate the relative stabilities of different states (Smith, 1998; Young and Smith, 2000; Smith et al., 2004; Whitley and Smith, 2004). Nevertheless, it should be clarified that in experiments of clay hydration, vapor pressures are usually controlled (i.e. fixed chemical potential of water), but our strategy is performing a series of NPT simulations (fixed water contents) to find the possible hydrate states, which thence can be viewed to be proper approximations of the "truly" stable states. Because all the global minima of calculated immersion energy occur at water content of about 110 mg_{water}/g_{clay} (Fig. 3), the hydrated states with such water content should be the thermodynamically most favorable ones, in which one clay unit cell contains 5 water molecules approximately, i.e. a full water monolayer (Skipper et al., 1995a,b). There is no minimum present at lower water contents than 110 mg_{water}/g_{clay}, which suggests that no stable hydration state can exist with less water than a full monolayer in water-rich environments. This finding is quite different from the previous inference that a partial monolayer can stabilize Cs-smectites with only 1.2∼1.4 water molecules per unit cell (Calvet, 1972; Sutton and Sposito, 2001).

We find another local minimum on each immersion energy curve at about 220 mg_{water}/g_{clay}, which indicates the possible occurrence of double layer hydrates. This has also been reported in previous simulations (Smith, 1998; Whitley and Smith, 2004). But, no experiment has detected such a double layer hydrate of Cs-smectite (Calvet, 1972; Bérend et al., 1995). According to our simulation, it is deduced that the high energy barrier between 110 and 160 mg_{water}/g_{clay} (about 15 J/g_{clay}) may inhibit the continuous swelling to

Table 2
Comparison of simulated and experimentally measured basal spacings

Water content [mg_{water}/g_{clay}]	Sim. [Å]			Exp.[Å]
	Ari	Wyo	Bei	
0	10.39 ± 0.07	10.46 ± 0.13	10.42 ± 0.12	$10.7 \sim 11.5$[a]
80	12.11 ± 0.11	12.30 ± 0.12	12.35 ± 0.15	12.2[b]
110	12.60 ± 0.15	12.65 ± 0.15	12.80 ± 0.15	12.9[b]

[a] Calvet (1973); Bérend et al. (1995).
[b] (Mooney et al., 1952b; Calvet, 1973; Bérend et al., 1995; Chiou and Rutherford (1997).

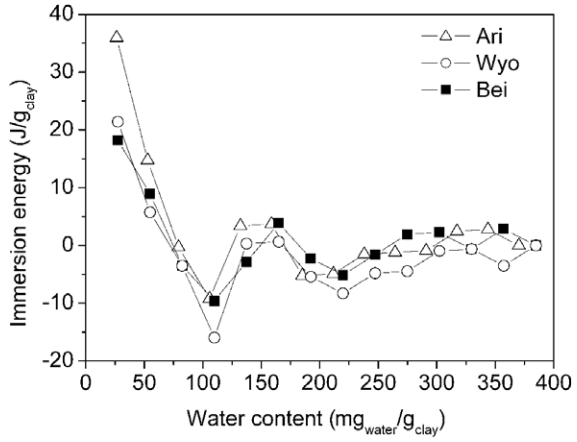

Fig. 3. Simulated immersion energy curves of the three Cs-smectites.

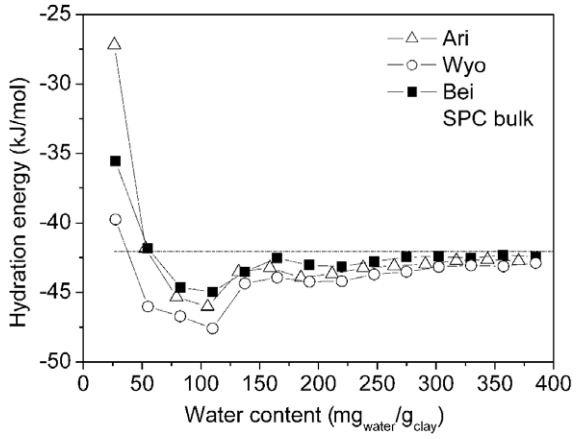

Fig. 4. Simulated hydration energy curves of the three Cs-smectites. The dotted horizontal line corresponds to the bulk energy of SPC water.

double layer hydrate. Additionally, the profiles of immersion energy (Fig. 3) are similar to that of K-smectite, but different from that of Na-smectite (Liu and Lu, 2006). In the case of Na-smectite, the global minimum of the hydration energy curve also occurs at low water content but the immersion energy curve presents the global minimum at a higher water content corresponding to the more expanded double-layer state. This reflects the difference of Cs^+ and Na^+: the former is a clay-swelling inhibitor analogous to K^+, but the latter is a promoter.

3.2. Interlayer structures

Fig. 5 shows the density profiles of interlayer water and ions, which are averaged over the two interlayer regions of the simulated models. In the cases of low water contents (Fig. 5(D) and (F)), water molecules are arranged in monolayers according to the mono-peak shape of density profiles except very slight splits observed for Wyo and Bei at about 110 mg_{water}/g_{clay}. As water content increases to 380 mg_{water}/g_{clay}, water molecules tend to form four layers in the space between two opposite clay layers (Fig. 5(B)).

In all cases, ions always locate at about 2.2∼2.5 Å away from clay surfaces (the range of 0∼3.28 Å on the distance axis in Fig. 5 stands for half a clay sheet). This distance range is very close to a recent measurement of Cs ion on the muscovite (001) plane, which gives the range of 2.15∼2.16 Å (Schlegel et al., 2006). Differently, for Wyo and Bei with water content of 380 mg_{water}/g_{clay}, Cs ions present relatively high probabilities occurring in the farther regions from the surfaces, whereas the Cs ions of Ari smectites can hardly escape from the surfaces (Fig. 5(A)). In addition, asymmetries are present in the cases of Ari at the two lower water contents (Fig. 5(C) and (E)). The ions tend to compensate the layer charges from both sides of clay sheet, so the full symmetries of the density profiles are not necessary (Chang et al., 1995, 1998).

The inner-sphere complex structures of binding Cs ions are very similar in different smectites. Taking the monolayer hydrate of Wyo with the water content of 110 mg_{water}/g_{clay} as an example, Fig. 6 shows the snapshots taken from the simulation trajectories. It can be seen that the distance of Cs-water is around 3.0 Å and the distance of Cs-basal oxygen ranges from 3.5 to 3.8 Å. In these binding structures, Cs ion contacts the clay surface directly and the surrounding water molecules form a cage-like cap over the ion. Such coordination environments are exactly analogous to those found in the K-smectites (Park and Sposito, 2002; Liu and Lu, 2006). Therefore, it is proposed that these complexes may be typical coordination structures of surface-preferring metal ions binding on basal surfaces of phyllosilicates.

3.3. Mobility of interlayer species

The calculated self-diffusion coefficients of water are displayed in Fig. 7. The magnitudes of the total coefficients of smectites with water contents of 55 mg_{water}/g_{clay} (Fig. 7(A)) and 110 mg_{water}/g_{clay} (Fig. 7(B)) are about 10^{-10}, much

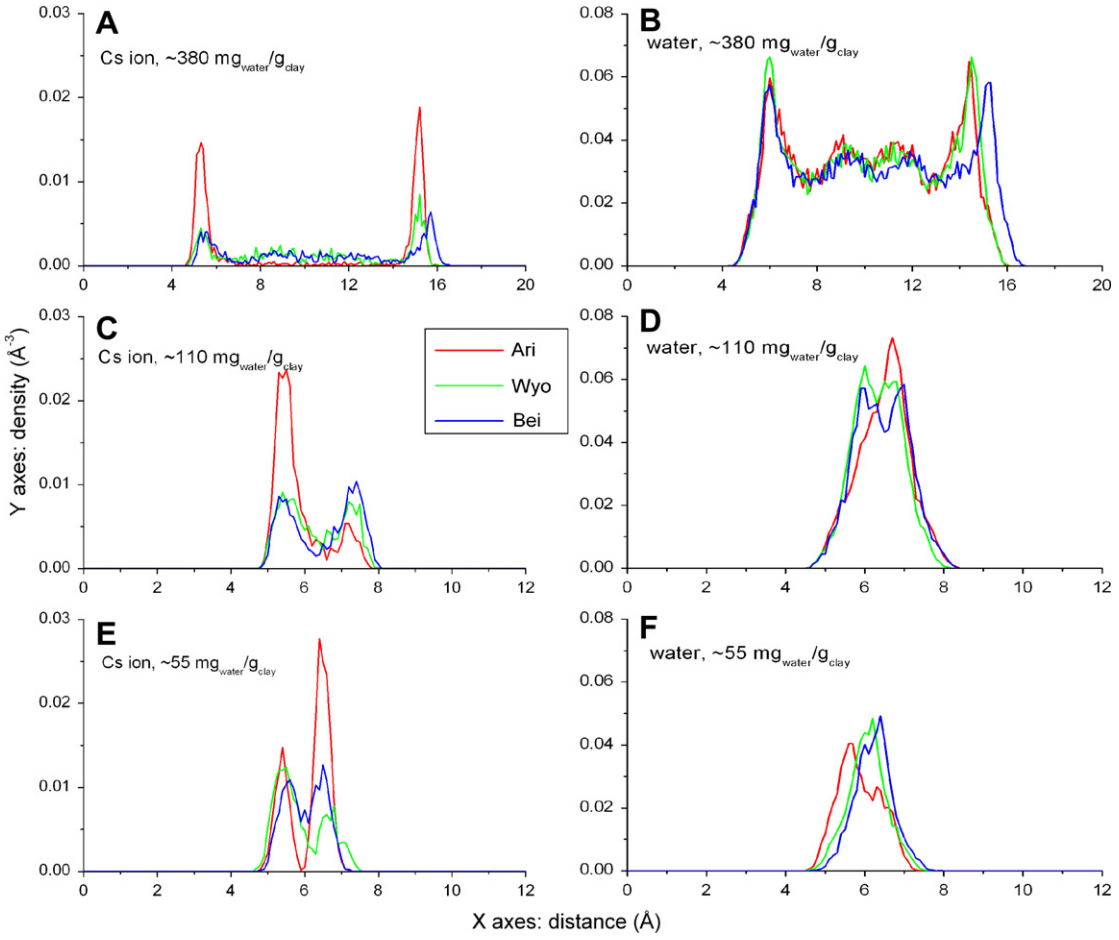

Fig. 5. Density profiles of Cs (left) and water (right) in the interlayer spaces of Ari, Wyo and Bei.

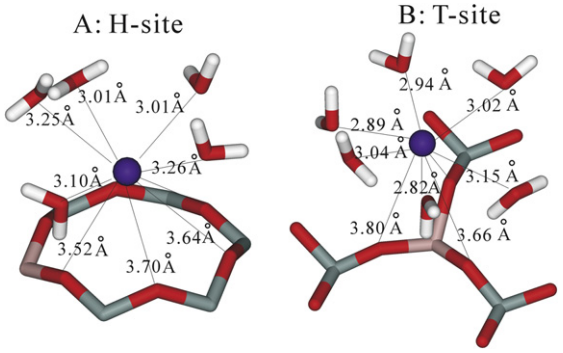

Fig. 6. Local coordination environments of Cs ion on (A) H-site and (B) T-site. Cs = purple, O = red, H = white, Si = grey and Al = faded pink. (For interpretation of the references to color in this figure legend, the reader is referred to the web version of this paper.)

lower than that of the bulk value (2.3×10^{-9} m^2/s) (Ohtaki and Radnai, 1993). The coefficients increase with water contents and get close to the bulk value at 380 mg$_{water}$/g$_{clay}$ (Fig. 7(C)). It is also clear that the diffusion along the z axis are negligible for the three smectites at all water contents, whereas the coefficients of the diffusion parallel to (0 0 1) plane are much larger.

Fig. 8(A) illustrates the MSDs of Cs ions in the three smectites at 55 mg$_{water}$/g$_{clay}$, which cannot be fitted with Eq. (6). These MSD data show that the motions of ions are in fact below the detectable limits (Skipper et al., 1993), and thence no macroscopic diffusions can be defined. So the ions can be viewed to be stationary with this water content. This shows that all the three smectites can fix Cs ions effectively at relatively dry conditions. At 110 mg$_{water}$/g$_{clay}$, the three total coefficients are two orders of magnitude lower than that of the bulk solution (2.0×10^{-9} m^2/s) (Nye, 1979) and at the same time the ZZ components are extremely low. At 380 mg$_{water}$/g$_{clay}$, all of the total coefficients increase obviously and those of Wyo and Bei reach the same magnitude with the bulk value. Interestingly, the ZZ components of Wyo and Bei increase obviously in the simulation time span, whereas that of Ari still remains trivial. Notably, the ion mobility in Ari is the lowest among the three smectites at both high and low water contents. For both water and ions in all cases, the observation that the ZZ coefficients are much lower than the corresponding (XX+YY)/2 components can be attributed to the confining effect of the clay surfaces: the constrained geometry of clay pore limits the movement in the z direction whereas the direction in x–y plane is relatively open (Skipper et al., 2006).

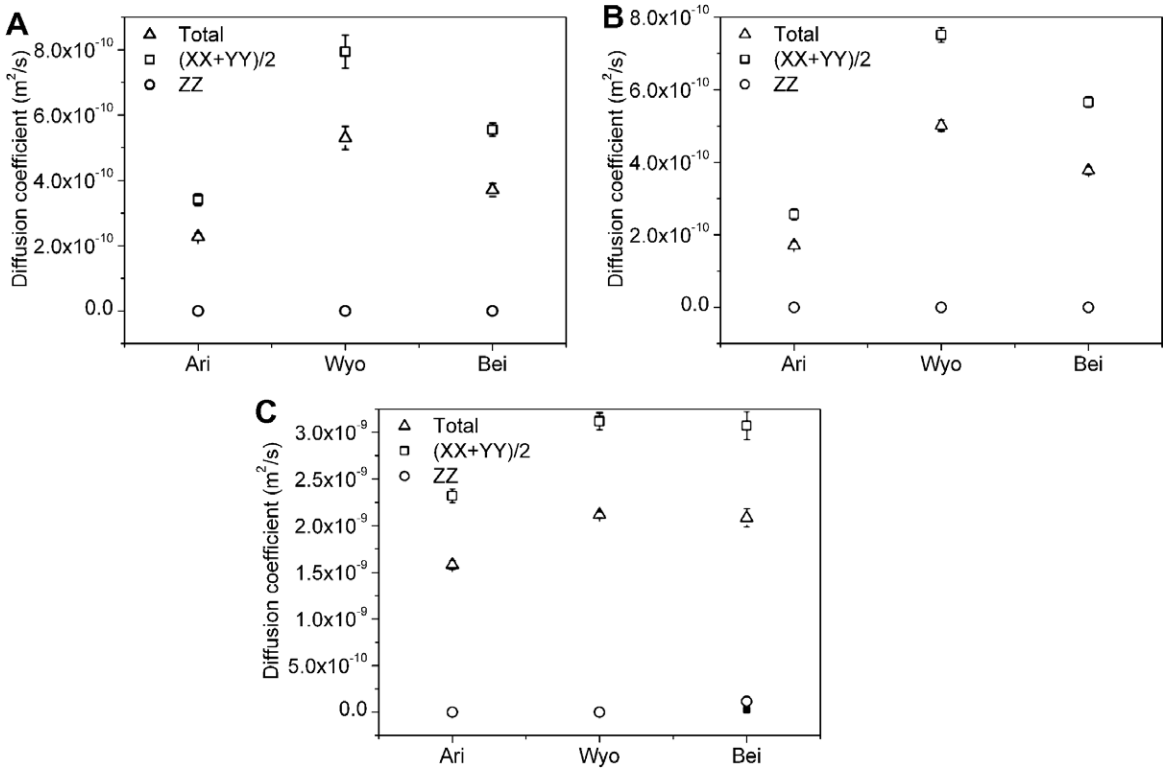

Fig. 7. Self-diffusion coefficients of water in the simulated Cs-smectites. The water contents are (A) 55 mg_{water}/g_{clay}, (B) 110 mg_{water}/g_{clay} and (C) 380 mg_{water}/g_{clay}. The separate contribution on each direction is denoted by XX, YY, and ZZ. The term "(XX+YY)/2" stands for the contribution of the movement parallel to the *x*-*y* plane.

3.4. Distributions of Cs binding sites

Fig. 9 shows the distributions of ion binding sites at the three water contents, where the total sites are represented in grey. In the data of Ari and Wyo, it is found that the percent of H_o occupation is always almost equal to that of H_n binding, i.e. the octahedral substitutions cannot improve the preference level of H-site. So, in Fig. 9 the occupied H_o and H_n amounts are combined together and noted as "H_n" for purpose of clarity.

Fig. 9 shows that in Ari with the three water contents, Cs ions always locate above H-sites and never occur above T-sites. In Wyo and Bei, ions can bind to both types of sites and more T-sites are occupied in Wyo than in Bei. With the water content of 380 mg_{water}/g_{clay} (Fig. 9 (C)), more ions can move away from the surfaces in Wyo and Bei than in Ari, that is consistent with the corresponding density profiles (Fig. 5).

It is indicated that both energetic and geometric factors make H-site preferable to the T-site. While T-sites being two times more than H-sites in the three smectites, much more H-sites are occupied than the former (Fig. 9(A)–(C)), it is deduced that H-sites are always preferable to T-sites. Furthermore, in Wyo and Bei, while H_t is much less than H_n, there are more H_t-sites occupied than H_n-sites. Hence, H_t is preferable to H_n. In a similar way, we can also know that T_t is preferable to T_n, too. In short, the relative preferable site of ion binding follows the order of $H_t > H_n > T_t > T_n$. This sequence has an atomic origin. Firstly, Cs ion above the H-site interacts with six hexagonal oxygen atoms simultaneously, whereas it interacts with only three bridging oxygen atoms above the T-site (Fig. 6). Secondly, the tetrahedral silicon atom (about 0.5 Å below the T-site) must repulse the ion more strongly than the structural hydroxyl (about 2.3 Å below the H-site). Thirdly, the larger area of H-site (17.5 $Å^2$) than T-site (3.4 $Å^2$) also makes H-site superior to stabilize Cs ion. Fourthly, based on molecular orbital study, Ebina et al. (1999) found that Cs adsorption energy on H-site is lower than that on T-site. These supportive evidences confirm the preference of H-sites over T-sites. The aluminum atom of T_t-site is less positive than the silicon of T_n (1.575*e* vs. 2.1*e*), and the three bridging oxygen atoms are a little more negative than the bridging oxygen of T_n (−1.1688*e* vs. −1.05*e*) (Cygan et al., 2004b). This makes T_t-site more accessible for Cs ion than the T_n-site (also explaining H_t is preferable to H_n in Wyo and Bei). Accordingly, ions can never bind to the T-sites in Ari as no T_t-site present, but they do bind to T-sites in Wyo and Bei as T_t-sites exist (Fig. 9). Subsequently, Cs ion on T-site is more mobile than on H-site, and thence the least T-site occupations in Ari lead to the lowest ion mobility. More T-site bindings in Wyo (Fig. 9(B)) are responsible for the highest mobility of Cs ions (Fig. 8(B)). This makes Cs ions in Wyo and Bei more possibly migrate away from the clay surfaces at higher water content (Fig. 8(C) and Fig. 5(A)) and enter the diffuse layer easily.

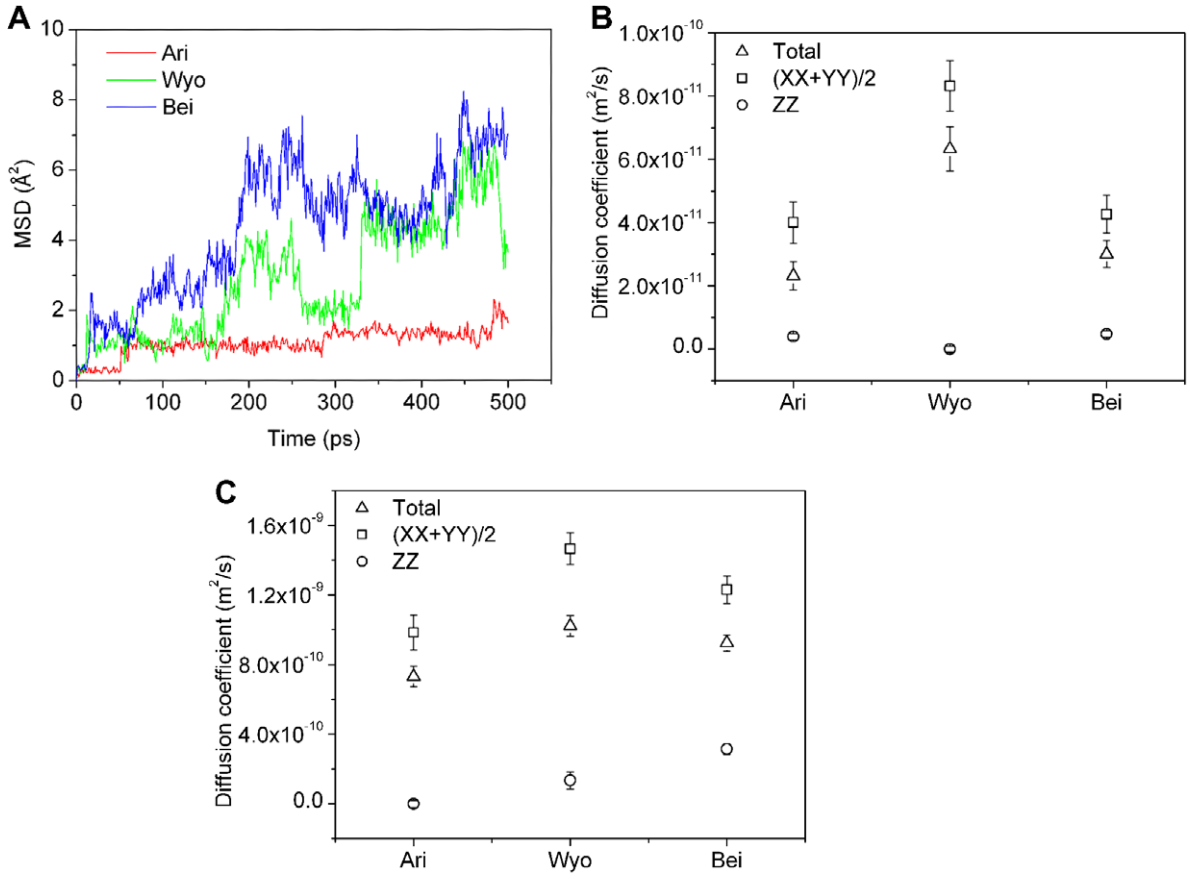

Fig. 8. Mobility of Cs ions. (A) MSDs of Cs ions in the three smectites with water content of 55 mg_{water}/g_{clay}. Self-diffusion coefficients of ions at water content of 110 mg_{water}/g_{clay} (B) and 380 mg_{water}/g_{clay}(C).

The site-preference sequence can be used to qualitatively predict binding behavior of the cations and positively charged headgroups of organic matters binding to negatively charged clay surface. For example, it is found that ammonium cations always bind to H-sites rather than T-sites in organo-clay nanocomposite (Greenwell et al., 2005; Liu et al., 2007). Furthermore, this finding can be easily applied to other phyllosilicate members. Because the interaction with solvents is ignored in above discussion, it should be emphasized that this sequence is useful particularly for surface-preferring ions (e.g. K^+, Cs^+), but less meaningful for easily hydratable ions (e.g. Na^+, Ca^{2+}), which usually tend to escape from the clay surface and form outer-sphere complexes or diffuse ions (Sposito and Prost, 1982; Sposito et al., 1999; Liu and Lu, 2006).

3.5. Implications for Cs fixation

Current simulations show that on one hand the H-site rather than the T-site favors Cs-fixation, on the other hand, the unique swelling behavior of smectites increases the opportunity for ions to enter interlayer spaces and contact more clay surfaces. These explain why smectites are very suitable to be used as buffer materials in practice. It is also suggested that both nonswelling phyllosilicates (e.g. pyrophyllite) and some swelling ones with higher fraction of tetrahedral charges (e.g. vermiculite) cannot fix Cs ions satisfactorily. Because the layer-charge distributions of smectites from different mines differ from each other (Yariv and Michaelian, 2002), evaluation of the characteristic of layer-charge distribution and selection of the raw clays with higher octahedral charge fraction become important for application of buffer materials. Additionally, the simulations show that all smectites effectively immobilize Cs in dry conditions, so predrying the barrier materials could improve the efficiency of Cs fixation.

The current study has simulated the behaviors of Cs-smectites under near-surface conditions with initial motives to mimic the environmental realities of low-level and intermediate-level nuclear waste disposal sites (Kittel, 1989). However in deep geological disposal of the high-level nuclear waste, both higher pressure and higher temperature have most likely nonnegligible effects on the behavior of smectites, and the influences of radiation of the high-level nuclear wastes on the crystallinity of contact minerals are found to be significant (Farnan et al., 2007). Under such conditions, some properties of smectites may change accordingly (Odriozola et al., 2004), which calls for further studies.

4. CONCLUSIONS

Molecular dynamics simulations provide comprehensive insights into effects of layer-charge distribution on various properties of Cs-smectites, including swelling behaviors,

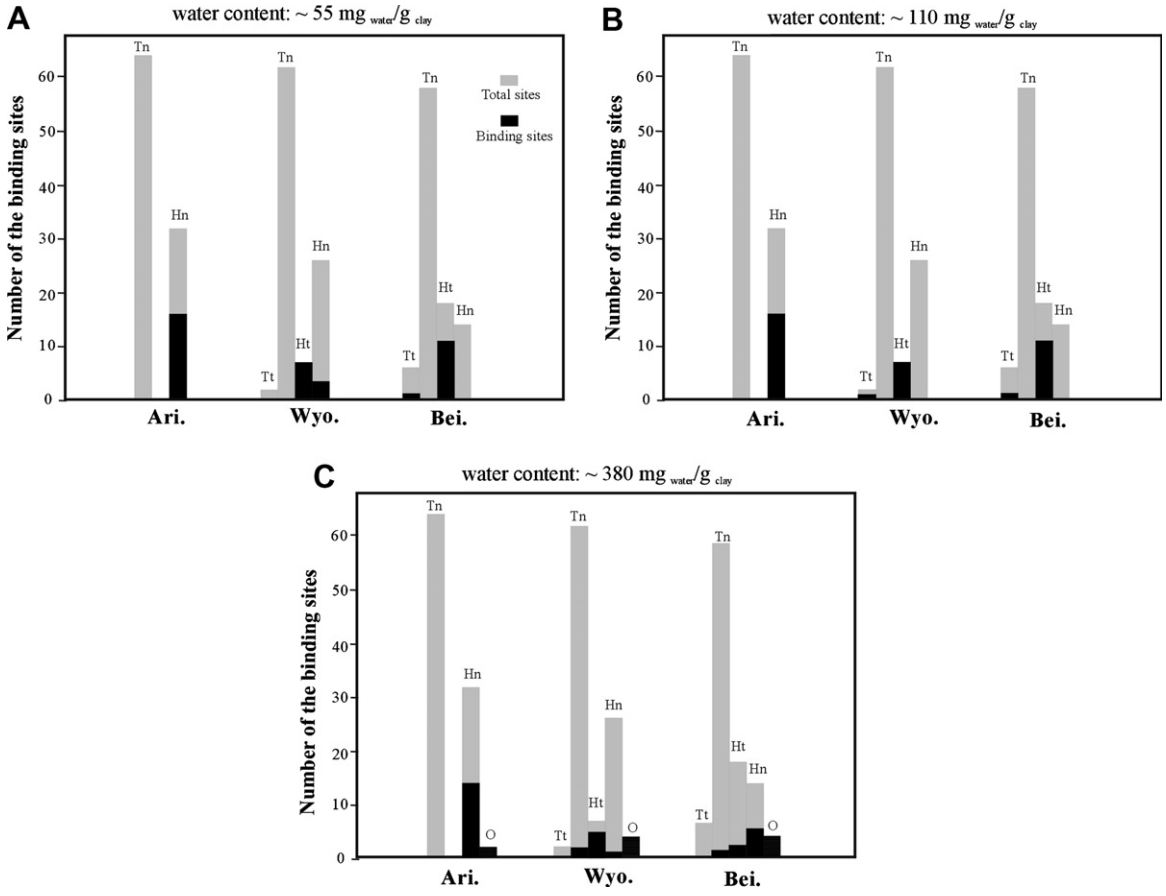

Fig. 9. Distributions of Cs ion binding sites in the simulated smectites with water contents of (A) 55 mg_{water}/g_{clay}, (B) 110 mg_{water}/g_{clay} and (C) 380 mg_{water}/g_{clay}.

ion binding sites, distributions and mobility of interlayer species. The new advances of this study include:

(1) Layer-charge distribution has negligible influence on the swelling behaviors of Cs-smectites. Under ambient conditions, the most stable swelling state of Cs-smectite corresponds to the full-monolayer hydrate with water content of about 110 mg_{water}/g_{clay}.
(2) Layer-charge distribution has obvious effects on the mobility of interlayer species. The smectite with the highest octahedral charges has the lowest ion mobility at both high and low water contents, which is much lower than the corresponding bulk case.
(3) Layer-charge characteristic significantly influences the distribution of Cs^+ binding sites: the H-sites are preferable to the T-sites, and tetrahedral substitutions can enhance the preferences of both types of sites, whereas octahedral substitutions cannot obviously improve the preference level of H-sites. This conclusion is extendable to the adsorption of other surface-preferring ions on 2:1 type phyllosilicates. The inner-sphere complex structures of Cs^+ are very similar in different smectites: ions bind on the H-sites or T-sites and surrounding water molecules form cage-like caps covering the ions.
(4) All types of smectites can fix Cs ions in relatively dry conditions and the smectite with higher octahedral charge fraction is more effective barrier material without dependence on water content.

ACKNOWLEDGMENTS

The authors acknowledge Rustad J.R. and two anonymous reviewers for their constructive comments. Authors gratefully thank the National Science Foundation of China (No. 40673041) and the Scientific Research Foundation of Graduate School of Nanjing University. Authors also acknowledge Dr. Hu Huan for her valuable advice.

REFERENCES

Allen M. P. and Tildesley D. J. (1987) *Computer Simulation of Liquids*. Clarendon Press, Oxford, UK.

Bérend I., Cases J. M., François M., Uriot J. P., Michot L., Masion A. and Thomas F. (1995) Mechanism of adsorption and desorption of water vapor by homoionic montmorillonites: 2. The Li^+, Na^+, K^+, Rb^+ and Cs^+-exchanged forms. *Clays Clay Miner.* **43**, 324–336.

Berendsen H. J. C., Postma J. P. M., van Gunsteren W. F. and Hermans J. (1981) Interaction models for water in relation to

protein hydration. In *Intermolecular Forces* (ed. B. Pullman). Riedel, Dordrecht, The Netherlands, p. 331.

Bleam W. F. (1993) Atomic theories of phyllosilicates: Quantum chemistry, statistical mechanics, electrostatic theory, and crystal chemistry. *Rev. Geophys.* **31**, 51–74.

Boek E. S., Coveney P. V. and Skipper N. T. (1995) Monte Carlo molecular modelling studies of hydrated Li-, Na-, and K-smectites: understanding the role of potassium as a clay swelling inhibitor. *J. Am. Chem. Soc.* **117**, 12608–12617.

Bostick B. C., Vairavamurthy M. A., Karthikeyan K. G., Chorover J. and Jonchorover (2002) Cesium adsorption on clay minerals: an EXAFS spectroscopic investigation. *Environmental Science & Technology* **36**, 2670–2676.

Brindley G. W. and Brown G. (1980) *Crystal Structures of Clay Minerals and their X-ray Identification*. Mineralogical Society, London.

Calvet R. (1972) Adsorption de l'eau sur les argiles; étude de. l'hydratation de la montmorillonite. *Bull. Soc. Chim. France* **8**, 3097–3104.

Calvet R. (1973) Hydratation de la montmorillonite et diffusion des cations compensateurs. I. Saturation par des cations monovalents. *Ann. Agron.*, 77–133.

Chang F.-R. C., Skipper N. T. and Sposito G. (1995) Computer simulation of interlayer molecular structure in sodium montmorillonite hydrates. *Langmuir* **11**, 2734–2741.

Chang F.-R. C., Skipper N. T. and Sposito G. (1997) Monte Carlo and molecular dynamics simulations of interfacial structure in lithium-montmorillonite hydrates. *Langmuir* **13**, 2074–2082.

Chang F.-R. C., Skipper N. T. and Sposito G. (1998) Monte Carlo and molecular dynamics simulations of electrical double-layer structure in potassium montmorillonite hydrates. *Langmuir* **14**, 1201–1207.

Chávez-Páez M., van Workum K., de Pablo L. and de Pablo J. J. (2001) Monte Carlo simulations of Ca-montmorillonite hydrates. *J. Chem. Phys.* **114**, 1405–1413.

Chiou C. T. and Rutherford D. W. (1997) Effects of exchanged cation and layer charge on the sorption of water and EGME vapors on montmorillonite clays. *Clays Clay Miner.* **45**, 867–880.

Cho W. J., Oscarson D. W., Gray M. N. and Cheung S. C. H. (1993) Influence of diffusant concentration on diffusion coefficients in clay. *Radiochim. Acta* **60**, 159–163.

Cornell R. M. (1993) Adsorption of cesium on minerals: a review. *J. Radioanal. Nucl. Chem.* **171**, 483–500.

Cygan R. T., Guggenheim S. and van Groos A. F. K. (2004a) Molecular models for the intercalation of methane hydrate complexes in montmorillonite clay. *J. Phys. Chem. B* **108**, 15141–15149.

Cygan R. T., Liang J. J. and Kalinichev A. G. (2004b) Molecular models of hydroxide, oxyhydroxide, and clay phases and the development of a general force field. *J. Phys. Chem. B* **108**, 1255–1266.

Ebina T., Iwasaki T., Onodera Y. and Chatterjee A. (1999) A comparative study of DFT and XPS with reference to the adsorption of caesium ions in smectites. *Comput. Mater. Sci.* **14**, 254–260.

Evans D. W., Alberts J. J. and Clark R. A. (1983) Reversible ion-exchange fixation of cesium-137 leading to mobilization from reservoir sediments. *Geochim. Cosmochim. Acta* **47**, 1041–1049.

Farnan I., Cho H. and Weber W. J. (2007) Quantification of actinide a-radiation damage in minerals and ceramics. *Nature* **445**, 190–193.

Frenkel D. and Smit B. (1996) *Understanding Molecular Simulation*. Academic Press, San Diego, CA.

Greathouse J. A. and Cygan R. T. (2005) Molecular dynamics simulation of uranyl(VI) adsorption equilibria onto an external montmorillonite surface. *Phys. Chem. Chem. Phys.* **7**, 3580–3586.

Greenwell H. C., Harvey M. J., Boulet P., Bowden A. A., Coveney P. V. and Whiting A. (2005) Interlayer structure and bonding in nonswelling primary amine intercalated clays. *Macromolecules* **38**, 6189–6200.

Grim R. E. (1962) *Applied Clay Mineralogy*. McGraw-Hill, New York.

He H. P., Galy J. and Gerard J. F. (2005) Molecular simulation of the interlayer structure and the mobility of alkyl chains in HDTMA(+)/montmorillonite hybrids. *J. Phys. Chem. B* **109**, 13301–13306.

Karaborni S., Smit B., Heidug W., Urai J. and Van Oort E. (1996) The swelling of clays: molecular simulations of the hydration of montmorillonite. *Science* **271**, 1102–1104.

Kim Y., Cygan R. T. and Kirkpatrick R. J. (1996) ^{133}Cs NMR and XPS investigation of cesium adsorbed on clay minerals and related phases. *Geochim. Cosmochim. Acta* **60**, 1041–1052.

Kirkpatrick R. J., Kalinichev A. G., Hou X. and Struble L. (2005) Experimental and molecular dynamics modeling studies of interlayer swelling: water incorporation in kanemite and ASR gel. *Mater. Struct.* **38**, 449–458.

Kittel J. H. (1989) *Near-surface land disposal*. Harwood Academic Publishers, New York.

Liu X. D. and Lu X. C. (2006) A thermodynamic understanding of clay-swelling inhibition by potassium ions. *Angew. Chem., Int. Ed.* **45**, 6300–6303.

Liu X. D., Lu X. C., Wang R. C., Zhou H. Q. and Xu S. J. (2007) Interlayer structure and dynamics of alkylammonium-intercalated smectites with and without water: a molecular dynamics study. *Clays Clay Miner.* **55**, 554–564.

Loewenstein W. (1954) The distribution of aluminum in the tetrahedra of silicates and aluminates. *Am. Mineral.* **39**, 92–96.

Masashi N., Katsuyuki K. and Yasuaki I. (2003) Local structural information of Cs in smectite hydrates by means of an EXAFS study and molecular dynamics simulations. *Appl. Clay Sci.* **23**, 15–23.

Mooney R. W., Keenan A. G. and Wood L. A. (1952a) Adsorption of water vapor by montmorillonite. I. Heat of desorption and application of BET theory. *J. Am. Chem. Soc.* **74**, 1367–1371.

Mooney R. W., Keenan A. G. and Wood L. A. (1952b) Adsorption of water vapor by montmorillonite. II. Effect of exchangeable ions and lattice swelling as measured by X-ray diffraction. *J. Am. Chem. Soc.* **74**, 1371–1374.

Nye P. H. (1979) Diffusion of ions and uncharged solutes in soils and soil clays. *Adv. Agron.* **31**, 225–272.

Odriozola G., Aguilar J. F. and Lopez-Lemus J. (2004) Na-montmorillonite hydrates under ethane rich reservoirs: $NP_{zz}T$ and $\mu P_{zz}T$ simulations. *J. Chem. Phys.* **121**, 4266–4275.

Ohtaki H. and Radnai T. (1993) Structure and dynamics of hydrated ions. *Chem. Rev.* **93**, 1157–1204.

Onodera Y., Iwasaki T., Ebina T., Hayashi H., Torii K., Chatterjee A. and Mimura H. (1998) Effect of layer charge on fixation of cesium ions in smectites. *J. Contamin. Hydrol.* **35**, 131–140.

Park S.-H. and Sposito G. (2002) Structure of water adsorbed on a mica surface. *Phys. Rev. Lett.* **89**, 85501.

Plimpton, S. J. (1995) Fast parallel algorithms for short-range molecular dynamics. *J. Comp. Phys.* **117**, 1–19. The URL is <www.cs.sandia.gov/~sjplimp/lammps.html>.

Schlegel M. L., Nagy K. L., Fenter P., Cheng L., Sturchio N. C. and Jacobsen S. D. (2006) Cation sorption on the muscovite (0 0 1) surface in chloride solutions using high-resolution X-ray reflectivity. *Geochim. Cosmochim. Acta* **70**, 3549–3565.

Skipper N. T. (1998) Computer simulation of aqueous pore fluids in 2:1 clay minerals. *Mineral. Mag.* **62**, 657–667.

Skipper N. T., Chang F.-R. C. and Sposito G. (1995a) Monte Carlo simulation of interlayer molecular structure in swelling clay minerals. 1. Methodology. *Clays Clay Miner.* **43**, 294–303.

Skipper N. T., Chang F.-R. C. and Sposito G. (1995b) Monte Carlo simulation of interlayer molecular structure in swelling clay minerals. 2. Monolayer hydrates. *Clays Clay Miner.* **43**, 294–303.

Skipper N. T., Lock P. A., Titiloye J. O., Swenson J., Mirza Z. A., Howells W. S. and Fernandez-Alonso F. (2006) The structure and dynamics of 2-dimensional fluids in swelling clays. *Chem. Geol.* **230**, 182–196.

Skipper N. T., Refson K. and McConnell J. D. C. (1993). In *Geochemistry of Clay-Pore Fluid Interactions* (eds. D. C. Manning, P. L. Hall and C. R. Hughs). Chapman and Hall, London, Chapter 3.

Smith D. E. (1998) Molecular computer simulations of the swelling properties and interlayer structure of cesium montmorillonite. *Langmuir* **14**, 5959–5967.

Smith D. E., Wang Y. and Whitley H. D. (2004) Molecular simulations of hydration and swelling in clay minerals. *Fluid Phase Equilibria* **222**, 189–194.

Sposito G. and Prost R. (1982) Structure of water adsorbed on smectites. *Chem. Rev.* **82**, 553–573.

Sposito G., Skipper N. T., Sutton R., Park S.-H., Soper A. K. and Greathouse J. A. (1999) Surface geochemistry of the clay minerals. *Proc. Natl. Acad. Sci. USA* **96**, 3358–3364.

Sutton R. and Sposito G. (2001) Molecular simulation of interlayer structure and dynamics in 12.4 Å Cs-smectite hydrates. *J. Colloid Interface Sci.* **237**, 174–184.

Sutton R. and Sposito G. (2002) Animated molecular dynamics simulations of hydrated caesium-smectite interlayers. *Geochem. Trans.* **3**, 73–80.

Tambach T. J., Hensen E. J. M. and Smit B. J. (2004a) Molecular simulations of swelling clay minerals. *J. Phys. Chem. B* **108**, 7586–7596.

Tambach T. J., Bolhuis P. G. and Smit B. (2004b) A molecular mechanism of hysteresis in clay swelling. *Angew. Chem., Int. Ed.* **43**, 2650–2652.

Teleman O., Jonsson B. and Engstrom S. (1987) A molecular dynamic simulation of a water model with intramolecular degrees of freedom. *Mol. Phys.* **60**, 193–203.

Teppen B. J. and Miller D. M. (2006) Hydration energy determines isovalent cation exchange selectivity by clay minerals. *Soil Sci. Soc. Am. J.* **70**, 31–40.

Wang J. W., Kalinichev A. G. and Kirkpatrick R. J. (2004) Molecular modeling of water structure in nano-pores between brucite (0 0 1) surfaces. *Geochim. Cosmochim. Acta* **68**, 3351–3365.

Wang J. W., Kalinichev A. G. and Kirkpatrick R. J. (2006) Effects of substrate structure and composition on the structure, dynamics, and energetics of water at mineral surfaces: a molecular dynamics modeling study. *Geochim. Cosmochim. Acta* **70**, 562–582.

Weiss C. A., Kirkpatrick R. J. and Altaner S. P. (1990) Variations in interlayer cation sites of clay minerals as studied by ^{133}Cs MAS nuclear magnetic resonance spectroscopy. *Am. Mineral.* **75**, 970–982.

Whitley H. D. and Smith D. E. (2004) Free energy, energy, and entropy of swelling in Cs-, Na-, and Sr-montmorillonite clays. *J. Chem. Phys.* **120**, 5387–5395.

Yariv S. and Michaelian K. H. (2002) Structure and surface acidity of clay minerals. In *Organo-Clay Complexes and Interactions* (eds. S. Yariv and K. H. cross). Marcel Dekker, New York, pp. 1–38.

Young D. A. and Smith D. E. (2000) Simulations of clay mineral swelling and hydration: dependence upon interlayer ion size and charge. *J. Chem. Phys.* **104**, 9163–9170.

Associate editor: James R. Rustad